In-situ X-Ray Small Angle Scattering during the Crystallization of Amorphous $Mg_{76}Zn_{24}$

M. Schaal, P. Lamparter, and S. Steeb

Max-Planck-Institut für Metallforschung, Institut für Werkstoffwissenschaften, Stuttgart

Z. Naturforsch. **41 a,** 1123–1128 (1986); received June 30, 1986

By X-Ray small angle scattering the relaxation and crystallization of amorphous $Mg_{76}Zn_{24}$ was investigated in-situ. Radii of gyration of the different phases developing during the annealing of the sample were determined. By comparison of the small angle scattering results with DSC-results from the literature and the phase diagram the different phases could be identified. The crystallization of amorphous $Mg_{76}Zn_{24}$ is preceded by the formation of β-phase ($Mg_{72}Zn_{28}$)-like inhomogeneities in the amorphous phase. Further annealing leads to the final crystalline phases γ-MgZn and Mg.

1. Introduction

Amorphous Mg–Zn-alloys with about 70 a% Magnesium, i.e. alloys near the eutectic composition, were recently investigated concerning their wide angle scattering with X-Rays [1, 2] and neutrons [3], concerning their short range order with EXAFS [4, 5] and concerning their crystallization behaviour [6–10] with thermodynamic methods.

In the present work the medium range structure of amorphous $Mg_{76}Zn_{24}$ during relaxation – and crystallization – annealing treatment was investigated. We use X-Ray small angle scattering which generally provides information about regions with diameters between 10 and 10^3 Å, supposed they differ from their surroundings by the electron density. Up to now amorphous alloys such as $Cu_{75}Tb_{25}$ [11], Cu–Zr [12, 13 14], Cu–Ho [12], Cu–Y [12], Ni–Y [12], and $Fe_{81}Si_xB_{19-x}$ ($3 \leqq x \leqq 11$) [15] were investigated using this method.

2. Theoretical fundamentals

The coherent intensity $I(Q)$ scattered into the small angle region by a system of isolated regions of equal size in statistical arrangement can be calculated within the range $Q R_g < 1$ according to [16] as

$$I(Q) = I(0) \exp\{-\tfrac{1}{3} Q^2 R_g^2\} \tag{1}$$

with $Q = \left(\frac{4\pi}{\lambda}\right) \sin\theta$,

θ = half of the scattering angle,

λ = wavelength,

R_g = radius of gyration.

The radius of gyration is defined as second moment of the electron distribution:

$$R_g^2 = Z^{-1} \int \varrho(r) \cdot r^2 \, dV \tag{2}$$

with Z = Number of electrons per region,

$\varrho(r)$ = local number density of electrons,

r = coordinate within the region.

The integral in (2) extends over the volume of one region.

If the plot $\ln I(Q)$ versus Q^2 (Guinier-plot) yields a straight line then all the requirements for the validity of (1) are fulfilled, i.e. the system is a diluted system without mutual interferences between different regions. From the gradient m of the straight line we obtain

$$R_g = \sqrt{3m}. \tag{3}$$

If the regions are spherical with radius R_b, then

$$R_b = R_g \sqrt{5/3}. \tag{4}$$

If the system contains mainly two kinds of regions (1 and 2) then in analogy to (1), one has the relationship

$$I(Q) = I_1(0) \exp\{-\tfrac{1}{3} Q^2 R_{g1}^2\} + I_2(0) \exp\{-\tfrac{1}{3} Q^2 R_{g2}^2\}. \tag{5}$$

Reprint requests to Prof. Dr. S. Steeb, Max-Planck-Institut für Metallforschung, Institut für Werkstoffwissenschaften, Seestraße 92, 7000 Stuttgart 1.

0340-4811 / 86 / 0900-1123 $ 01.30/0. – Please order a reprint rather than making your own copy.

If the difference of two radii of gyration is large enough, then according to (5) we recognize two straight lines in the Guinier-plot which are well separated by a kink. If the difference between both radii of gyration is small, then we observe a broad region between the two straight lines in which the plot cannot be described by a straight line.

3. Experimental and results

3.1. Apparatus

Figure 1 shows the experimental arrangement [17]. The X-Rays emerge from the focus of a rotating X-Ray generator (type RU-200PL; Rigaku-Denki, Tokyo) with a power of maximum 12 kW (200 mA, 60 kV), copper anode, and optical focus of $10 \times 0{,}1\ mm^2$. The radiation is monochromatized by a bent graphite monochromator (Stoe, Darmstadt) and reaches the evacuated diffraction chamber through a window (Hostaphan 15 µm). Having passed through the water cooled Kratky system [18] the radiation is scattered by the specimen which is contained within a furnace. For further details see [19]. The Kratky system can be adjusted by the two micrometer screws 1 and 2 from outside the vacuum chamber. Using screw 3 the beam stop can be adjusted. The scattered intensity is detected by a position sensitive detector (PSD -50; Braun, Garching) with 11 to 14 bar pressure of the counting gas, a detector length of 50 mm and a resolution of 50 µm. The apparatus according to Fig. 1 allows to investigate specimens at temperatures up to 900 °C in the small angle- as well as in the wide angle-region (for CuKα: $10^{-2}\ Å^{-1} \leqq Q \leqq 5\ Å^{-1}$).

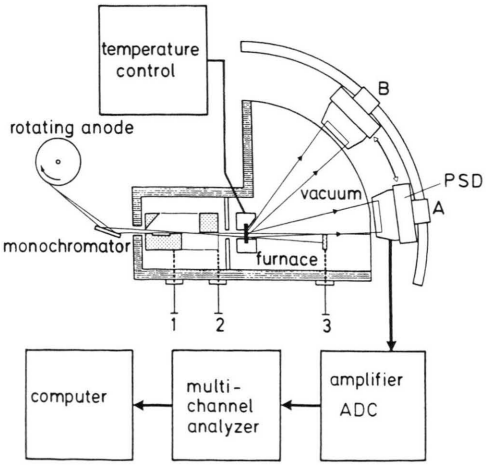

Fig. 1. Experimental arrangement.

3.2. Specimen preparation

Amorphous samples of the $Mg_{76}Zn_{24}$-alloy were produced by melt-spinning under 100 Torr Helium as ribbons with a width of 1 mm and a thickness of 40 µm. These ribbons were fixed in two layers within a cuvette. The thickness was larger by 17% than the optimum thickness $1/\mu$ for a transmission experiment with μ being the absorption coefficient. The density of the specimen amounts to $3.0\ g/cm^3$.

3.3. Diffraction experiment

For different reasons it is convenient and useful to perform relaxation- and crystallization-experiments using constant heating rates $\dot{T}$. By this procedure it becomes possible to apply existing theories to quantify the nucleation and grain growth in particular by the determination of the corresponding activation energies. To allow the discussion of the results of the present work in combination with the result of heat treatments performed elsewhere we also used constant $\dot{T}$. However, by this procedure difficulties arise since the recording of the intensity distribution takes a certain time. Preliminary experiments led to a convenient combination of exposure time = 1 hour and $\dot{T} = 0.375$ K/min.

3.4. Evaluation

The rough data were corrected for background scattering and then presented without smoothing as Guinier-plots as shown in Figs. 2 to 4. The numbers to the straight lines in these plots reappear in Table 1. In Tab. 1 the corresponding radii of gyration, the intersections $a = \text{const} \cdot \ln I\ (0)$ with the ordinate and the correlation coefficients Γ, which are a measure for the accordance between the experimental points and the straight line, are given.

Intervals as long as possible were chosen for the fit with straight lines in such a way that the resulting correlation coefficient Γ was as close as possible to one.

The comparison of the radii of gyration shows that they are in the order of 30 Å to 50 Å, which according to (4) correspond to radii R_b of spherical regions between 38 Å and 65 Å.

Table 1. $Mg_{76}Zn_{24}$; results of the Guinier evaluation in the different temperature ranges passed through during the heat treatment with $\dot{T} = 0.375$ K/min.

Run number	Designation of the straight lines	Temperature range [K]	Radius of gyration R_g [Å]	$\ln I(0)$	correlation coefficient Γ
1	1	294	40.5	0.97	0.999
2	2	294–315	34.3	−0.54	0.996
3	3	315–337	34.1	−1.34	0.989
4	4	361–385	33.0	−0.91	0.994
5	5	385–409	34.2	−0.48	0.995
6	6	409–434	35.1	0.03	0.999
7	7_1	434–458	47.3	2.39	0.994
	7_2		35.2	1.84	0.999
	7_3		29.4	1.22	0.997
8	8_1	458–482	37.8	2.29	0.998
	8_2		32.7	1.87	0.999
9	9_1	482–507	49.7	2.63	0.997
	9_2		37.7	2.15	0.999
10	10_1	507–529	51.1	1.85	0.994
	10_2		35.8	1.35	0.999
11	11_1	529–552	51.9	1.85	0.992
	11_2		38.9	1.35	0.999
12	12	552–575	38.9	1.14	0.997
13	13_1	575–598	50.9	1.47	0.995
	13_2		38.8	1.00	0.999
14	14_1	598–608	42.8	0.58	0.998
	14_2		34.1	−0.05	0.997

4. Discussion

4.1. Guinier-plots

The following four statements can be made as a result of the Guinier-plots in Figs. 2 to 4.

I) Between 294 K and 337 K the small angle scattering effect i.e. the total scattered intensity decreases and reaches a minimum with run 3 (see Figure 2).

II) Between 337 and 482 K the scattered intensity increases and reaches a maximum with run 8 (see Figure 3).

III) Between 482 K and 608 K the scattered intensity again decreases and reaches a minimum value just below the eutectic temperature (see Figure 4).

IV) The scattered intensity increases from run 6 (between 409 K and 434 K) to run 7 (between 434 K and 458 K) step-like by almost one order of magnitude (see Figure 3).

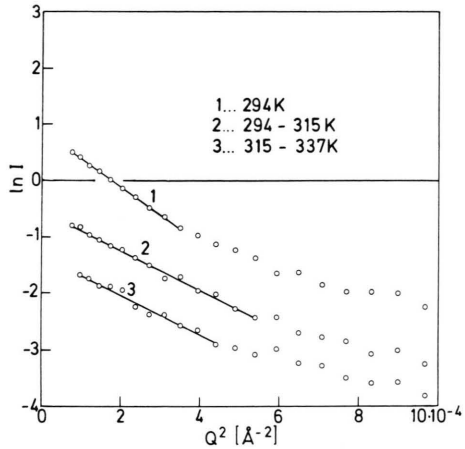

Fig. 2. Guinier-plots; runs 1 to 3; unsmoothed data.

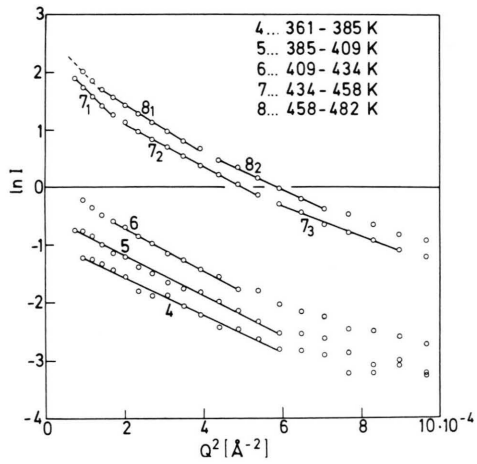

Fig. 3. Guinier-plots; runs 4 to 8; unsmoothed data.

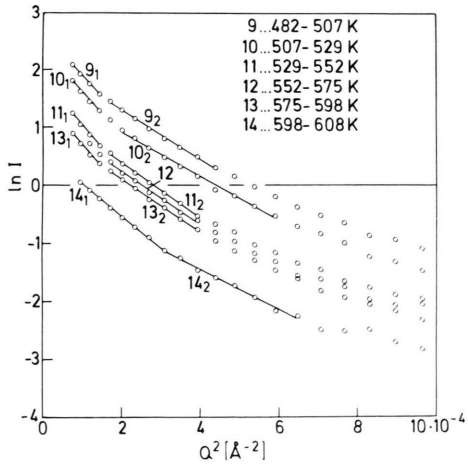

Fig. 4. Guinier-plots; runs 9 to 14; unsmoothed data.

4.2. Interpretation of the Guinier-plots

The evaluation of the Guinier-plots allows conclusions concerning the products formed within the specimen during the temperature treatment. The results obtained within the different temperature regions are discussed in the following.

i) **294 K up to 337 K** (run 1 to 3)

From Fig. 2 follows the existence of regions corresponding to the straight lines designed with 1, 2, 3. The decrease of $I(0)$ shows that the number of these inhomogeneities decreases accompanied by a decrease of the radii of gyration. Obviously the decrease of the total scattered intensity is due to a decrease of the electron density-fluctuations in the sample. As this effect is observed well below the crystallization temperature it must be associated with a relaxation process in the amorphous system where compositional fluctuations disappear.

ii) **337 K up to 482 K** (run 4 to 8)

Starting from the minimum of the total intensity represented by run 3 in Fig. 2 we observe a slight increase of the total scattered intensity with run 4 up to run 6. This increase suggests the appearance of a new phase. At run 7 a drastic increase of the intensity occurs which only can be explained by the appearance of a new phase with a large difference in electron density compared to that of the matrix or a large volume fraction of this phase. Furthermore, splitting into three kinds of regions with different radii of gyration (7_1, 7_2, 7_3) is indicated.

Since in Tab. 2 the intermetallic phase $Mg_{50}Zn_{50}$ shows the largest electron density, we assume that this phase causes the drastic increase of the intensity. The β-phase near the eutectic composition $Mg_{72}Zn_{28}$, however, shows a small difference in electron density compared to the starting substance $Mg_{76}Zn_{24}$. This suggests that this β-phase causes the slight increase of the intensity beginning with run 4.

Table 2. Electron densities [10^{23} e/cm^3].

Pure magnesium	Mg	5.17
Starting substance	$Mg_{76}Zn_{24}$	7.67
Eutectic composition β	$Mg_{72}Zn_{28}$	8.13
Intermetallic phase γ	$Mg_{50}Zn_{50}$	10.90

iii) **458 up to 608 K** (run 9 to 14)

The radii of gyration of the inhomogeneities increase up to 52 Å (see Table 1). At the same time the intensity decreases, most probably because the dimensions tend to become too large to be detectable in the Q-window of the present experimental set up. The growth of the large regions is correlated with a decrease in the number of the small regions, i.e. Ostwald-ripening occurs.

4.3. Temperature dependence of the radius of gyration

In Fig. 5 the radii of gyration R_g are plotted versus the temperature. In this Figure the temperature-behaviour of the R_g-values of the various reaction products can be seen.

The trace splits up beginning with run 7 into three traces. Between runs 7 and 8 the R_g's of the three traces show a sudden increase. The upper one corresponds to Mg and the two lower ones represent a range of the radii of gyration for the metastable γ^*-MgZn phase as explained below. The broken line within the Mg-trace corresponds to the broken line of run 8 in Figure 3. The corresponding R_g amounts

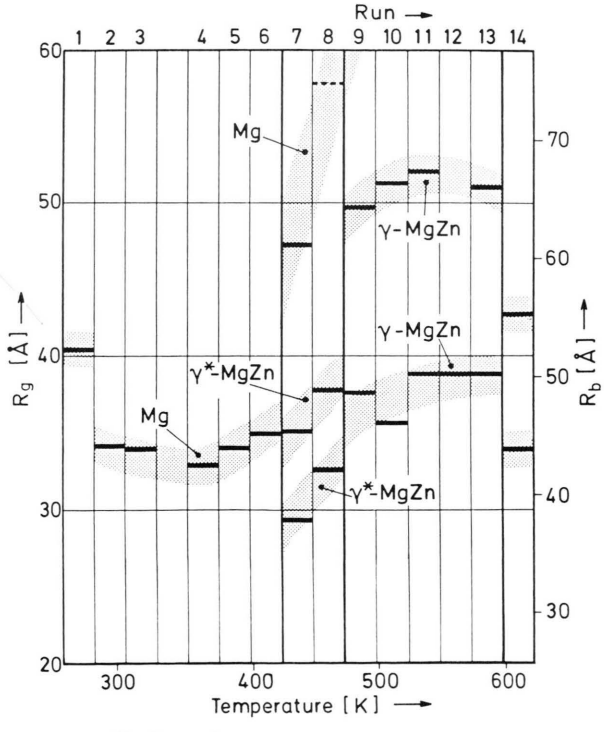

Fig. 5. Radii of gyration versus temperature.

to approximately 58 Å. However, for a confirmation of this value it is necessary to extend the experimental run in Fig. 3 to smaller Q-values. Between runs 9 and 13 the two traces for γ-MgZn are smooth. Run 14 yielded R_g's which cannot be ascribed to one of the two traces.

4.4. Crystallization process

Before crystallization starts, according to [10] Mg-rich inhomogeneities together with β-$Mg_{72}Zn_{28}$ already exist in amorphous Mg–Zn alloys. The increase of the small angle scattering effect from run 4 to 6 supports this tendency to phase separation into β-$Mg_{72}Zn_{28}$ and Mg-rich regions. According to the electron densities given in Table 2, for the element Mg a pronounced contrast compared to the starting substance is to be expected, whereas $Mg_{72}Zn_{28}$ inhomogeneities would yield a very small contrast. Thus the inhomogeneities observed in runs 4 to 6 must be attributed to Mg-regions.

Complete crystallization starts with run 7. During the crystallization the two phases Mg and γ*-MgZn are formed whose phase fields within the equilibrium phase diagram are shown in Figure 6 [20]. This reaction leads to a surplus of Mg which explains the jump of the Mg-trace in Fig. 5, run 7. The jump of the γ-MgZn-trace between run 8 and 9 hints to the transformation of the metastable γ*-phase to the stable γ-phase [10]. During run 14 an eutectoid reaction occurs which leads to the formation of Mg and of $Mg_{72}Zn_{28}$, i.e., the β-phase. The latter phase was originally designed as "Mg_7Zn_3". The structure of the β-phase was revealed in 1980 [21].

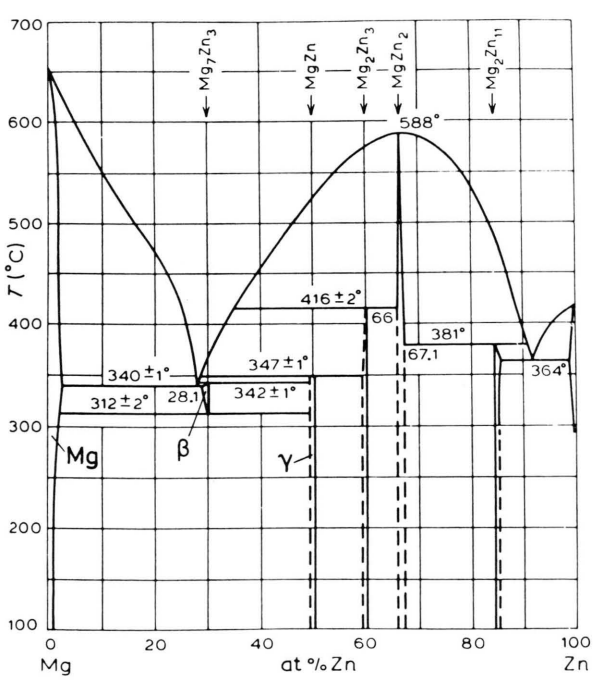

Fig. 6. Mg–Zn phase diagram [20].

4.5 Comparison with DSC-results and the phase diagram

With the Mg–Zn-system between 60 and 80 a% Mg amorphous alloys can be produced by rapid quenching. This concentration region was thoroughly studied by DSC-measurements [10]. These show the occurence of four exothermal reactions during the crystallization process of amorphous $Mg_{76}Zn_{24}$. The following correlations between total scattered intensities observed in the present work and the corresponding phases in [10] exist:

Starting from the
Minimum at 337 K: formation of Mg and β-$Mg_{72}Zn_{28}$,
Jump at 434 K: formation of Mg and metastable γ*-$Mg_{50}Zn_{50}$,
Maximum at 482 K: transformation to stable γ-$Mg_{50}Zn_{50}$,
Minimum at 598 K: formation of stable β-$Mg_{72}Zn_{28}$ with eutectic composition.

According to the phase diagram of the Mg–Zn-system [20] (Fig. 6) a melt containing 72 a% Mg solidifies mainly as stable β-phase. Further cooling leads at 585 K (312 °C) by an eutectoid reaction to the formation of the two phases Mg and γ-MgZn. The velocity of this reaction depends on the mobility of the atoms and therefore on the temperature. By rapid solidification of the β-phase the mobility of the atoms is reduced in such a way that this β-phase is preserved at room-temperature [21].

The fact that a melt with eutectic composition during solidification forms the β-phase and only small amounts of Mg is a hint on a structural relationship between the β-phase and the melt. The observation that annealing of the amorphous alloy $Mg_{76}Zn_{24}$ leads to the formation of the β-phase (besides Mg-regions) before onset of crystallization shows that the amorphous alloy during slow heating behaves similar to the corresponding melt during

slow solidification. This statement corresponds to one of the rules established by Khan et al. [22] for the crystallization of binary amorphous alloys which, therefore can very well be applied to the crystallization of the present Mg–Zn-alloy.

5. Summary

The relaxation and crystallization of amorphous $Mg_{76}Zn_{24}$ is investigated in-situ by means of X-Ray small angle scatttering. During the investigations the heating rate was kept constant at 0.375 K min^{-1}. The exposure time for each of the successive intensity diagrams was one hour. Radii of gyration are determined as well as the formation of various intermetallic phases starting from the moment of their formation. The time dependence of the radius of gyration is discussed together with DSC-measurements performed by other workers. As a result, the crystallization of amorphous $Mg_{76}Zn_{24}$ occurs via the β-phase ($Mg_{72}Zn_{28}$) to the final γ-phase. The β-phase is also formed by slowly cooling down a melt of the same composition. Thus the crystallization of an amorphous alloy and the solidification of a molten alloy proceed along the same intermediate steps (Khan's rule).

[1] H. Rudin, S. Jost, and J. Güntherodt, J. of Non-Crystalline Solids **61/62,** 291 (1984).
[2] E. Nassif, P. Lamparter, W. Sperl, and S. Steeb, Z. Naturforsch. **38a,** 142 (1983).
[3] P. Andonov and P. Chieux, J. Physique **46,** C 8–81 (1985).
[4] M. Ito, H. Iwasaki, N. Shiotani, H. Marumi, T. Mizoguchi, and T. Kawamura, J. Non-Crystalline Solids **61/62,** 303 (1984).
[5] A. Sadoc, R. Krishnan, and P. Rougier, J. Phys. F Met. Phys. **15,** 241 (1985).
[6] A. Calka, M. Madhava, D. E. Polk, B. C. Giessen, H. Matyja, and J. Van der Sande, Scripta Metallurgica **11,** 65 (1977).
[7] N. Shiotani, H. Narumi, H. Arai, K. Walkatsuki, Y. Sasa, and T. Mizoguchi, Proc. 4th Int. Conf. on Rapidly Quenched Metals Sendai (1981), p. 667.
[8] T. Matsuda and U. Mizutani, Proc. 4th Int. Conf. on Rapidly Quenched Metals Sendai (1981), p. 1315.
[9] I. Higashi, N. Shiotani, M. Uda, T. Mizoguchi, and J. Katoh, J. Solid State Chem. **36,** 225 (1981).
[10] Z. Altounian, T. Guo-Hua, and J. O. Strom-Olsen, J. Mat. Sci. **17,** 3268 (1982).
[11] B. Boucher, LAM4; J. Physique **41,** 135 (1980).
[12] A. M. Flank and A. Naudon, LAM4; J. Physique **41,** 123 (1980).
[13] P. Goudeau, J. C. Lasjaunias, A. Naudon, A. Ravex, and O. Bethoux, RQ 5 **1,** 663 (1985).
[14] M. Harmelin, A. Naudon, J. M. Frigerio, and J. Rivory, RQ 5 **1,** 659 (1985).
[15] G. Cocco, S. Enzo, C. Antonione, and G. Riontino, RQ 5 **1,** 303 (1985).
[16] A. Guinier, Ann. Physik **12,** 161 (1939).
[17] J. Höhler, Doctor Thesis, University of Stuttgart 1975.
[18] O. Kratky, Kolloid-Z. **144,** 110 (1955).
[19] M. Schaal, Diploma Thesis, University of Stuttgart 1985.
[20] R. P. Elliot, Constitution of Binary Alloys, First Supplement. McGraw-Hill, New York 1965.
[21] I. Higashi, N. Shiotani, M. Uda, T. Mizoguchi, and H. Katoh, J. Solid State Chem. **36,** 225 (1981).
[22] Y. Khan, E. Kneller, and M. Sostarich, Z. Metallkde. **72,** 553 (1981).